Computational Materials Science 45 (2009) 774–782

Contents lists available at ScienceDirect

Computational Materials Science

journal homepage: www.elsevier.com/locate/commatsci

Finite element crystal plasticity analysis of spherical indentation in bulk single crystals and coatings

O. Casals *, S. Forest

Centre des Matériaux, Mines ParisTech, CNRS UMR 7633, 91003 Evry Cedex, France

ARTICLE INFO

Article history:
Received 30 August 2008
Received in revised form 30 September 2008
Accepted 30 September 2008
Available online 26 November 2008

Keywords:
Micro-indentation
Crystal plasticity
Contact anisotropy
Coatings and thin films

ABSTRACT

The purpose of the present work is to investigate the anisotropy in the contact response of f.c.c and h.c.p single crystals. To this aim, spherical indentation experiments were simulated at a meso-scale, which is relevant to the interpretation of instrumented indentation experiments and micro-hardness tests in bulk single crystals and coatings. Within this framework, both the instrumented indentation load (P)-penetration depth (h_s) curves and the pile up or sinking-in patterns developed around the indentation imprint were analyzed. The detailed assessment of plastic zone morphology and plastic strain localization features was also addressed to complete the micro-mechanical analysis of indentation experiments. An important outcome from the present work is the identification of very specific and orientation dependent locations within the film–substrate interface, where plastic strain localizes as indentation proceeds. These findings can be significant on the prediction of delamination and potential failure of coatings and thin films.

1. Introduction

Mechanical property characterizations of small components and thin films are routinely performed using indentation techniques. Under the local contact solicitations developed during indentation experiments, only few micro-constituents, or even individual grains, actually rule the mechanical response of the component. Within this context, the classical macroscopic interpretation of indentation data may hardly apply due to the intrinsic anisotropy in both the elastic and plastic responses of single crystals. Hence, the use of continuum isotropic models and simplified power-law strain hardening relations, which are conventionally used for the analysis of indentation in polycrystalline metals [1–3] becomes at least debatable [4]. Alternatively, spherical indentation simulations can be performed within the framework of classical crystal plasticity models [5,6]. These constitutive models allow for the analysis of the intrinsic influence of the anisotropic plastic flow of different crystalline metals (i.e. f.c.c. copper and h.c.p. zinc single crystals) upon the contact response. It must be noted that the length scale under consideration is still large enough as to neglect any size effect associated to the nucleation and interaction of a reduced number of dislocations and to the activation of dislocation multiplication sources beneath the indenter. Hence, dislocation and molecular dynamics simulations, which are suitable for the numerical analysis of the contact yield point phenomenon [7] and ultra-low load nanoindentation experiments [8], remain out of the scope of the present research.

2. Computational method

2.1. Constitutive equations

In the present simulations, a fully anisotropic elasticity tensor was considered for modelling the elastic response of all single crystals (see Table 1). Furthermore, the crystal plasticity model initially proposed in [9] was used for the simulation of the corresponding plastic behavior. A large deformation formulation, accounting for finite strains and rotations, is adopted through the entire work since relatively large plastic strains are readily attained close to the contact zone. The kinematics of the model conform to the classical multiplicative decomposition of the deformation gradient

$$\mathbf{F} = \mathbf{F}^{\mathbf{e}}\mathbf{F}^{\mathbf{p}}, \tag{1}$$

whose plastic part, $\mathbf{F}^{\mathrm{p}}$, is assumed to be solely related to slip deformation occurring in discrete crystallographic slip systems characterized by unit vectors lying along the slip direction, $\mathbf{m}^{\mathbf{s}}$, and the normal to the slip plane, $\mathbf{n}^{\mathbf{s}}$.

$$\dot{\mathbf{F}}^{\mathrm{p}}\mathbf{F}^{\mathrm{p}\,-1} = \sum_{s=1}^{n} \dot{\gamma}^{s}\mathbf{m}^{\mathbf{s}} \otimes \mathbf{n}^{\mathbf{s}} \tag{2}$$

* Corresponding author.
E-mail addresses: ovidi.casals@ensmp.fr, ovidi.casals@compassis.com (O. Casals).

0927-0256/$ - see front matter © 2008 Elsevier B.V. All rights reserved.
doi:10.1016/j.commatsci.2008.09.030

Table 1
Anisotropic elastic properties of copper and zinc single crystals. All reported values are in MPa.

Copper (f.c.c)		Zinc (h.c.p.)			
C_{11}	159,300	C_{11}	165,000	C_{44}	33,475
C_{12}	122,000	C_{22}	165,000	C_{55}	19,800
C_{44}	81,000	C_{33}	61,800	C_{66}	19,800
				C_{12}	31,100
				C_{23}	50,000
				C_{31}	50,000

A rate dependent flow rule is adopted to facilitate the determination of a unique set of active slip systems [10]

$$\dot{\gamma}^s = \left\langle \frac{|\tau^s| - r^s}{K} \right\rangle^n \operatorname{sign}(\tau^s), \tag{3}$$

where τ^s is the resolved shear stress, r^s is the corresponding isotropic strain hardening variable, and K and n are viscosity parameters. A non-linear hardening rule, that governs the evolution of the hardening variable, completes the crystal plasticity constitutive model

$$r^s = r_o + q \sum_{r=1}^{n} h^{sr}(1 - \exp(-bv^r)), \tag{4}$$

In Eq. (4), r_o is the critical resolved shear stress, h^{sr} is a hardening matrix accounting for self ($r = s$) and latent ($r \neq s$) hardening, v^r is the cumulated plastic slip for system (r) and $\dot{v}^r = |\dot{\gamma}^r|$. Finally, q and b are phenomenological constants. Parameters for copper and zinc single crystals were taken from the literature [11–13] were different sets are proposed for best fitting experimental data obtained under different conditions (i.e. uniaxial tensile tests, cyclic loading, etc.). In the present work, the final set of parameters was chosen as to match, within reasonable accuracy, the anisotropic uniaxial behavior of the crystals while reproducing sensible hardness values during the simulation of indentation experiments. The anisotropic hardening behavior of Cu is enhanced by the heterogeneous hardening matrix h^{rs} taken for the $\{1\,1\,1\}\langle 0\,1\,1\rangle$ family of slip systems. Specifically, h_1 in Table 2 accounts for self-hardening (i.e. $s = r$) while $h_2 - h_6$ refer to the remaining independent components of latent-hardening. In this sense, in f.c.c crystals there only exist five distinct slip system interactions, leading to at most five independent components of the matrix. By contrast, anisotropy on Zn single crystals is mainly accounted for by the variety of plastic parameters adopted for different slip system families. In this case, the hardening matrix is assumed completely isotropic so that both self (h_1) and latent-hardening (h_2) are taken equal to unit in all slip system families. No additional interaction between different slip system families is considered.

In those simulations concerning indentation of thin films on hard substrates, a fully isotropic elastic response was assumed for modeling the substrate. Although this implies an important simplification on the actual behavior of the material, it is a suitable first approximation to the problem. A silicon substrate ($E = 150$ GPa) was considered for copper thin films, while a steel substrate ($E = 210$ GPa) was chosen in the case of zinc crystal thin films. These material combinations were taken for being representative of true systems that can be found in electronics and surface technology applications, respectively. In both cases the substrate is much harder than the coating, so it is expected that for even relatively large indentations the substrate may remain within its elastic regime.

Table 2
Crystal plasticity parameters for the distinct slip system families of copper and zinc single crystals.

	Cu (oct)	Zn (bas)	Zn (pyr)	Zn (pris)
K (MPa)	5.0	1.0	10.0	10.0
n	10.0	5.0	5.0	5.0
$r_\circ$ (MPa)	35.0	1.5	15.0	22.5
q (MPa)	6.0	1.0	15.0	22.0
b	15.0	3.0	30.0	10.0
h_1	1.0	1.0	1.0	1.0
h_2	4.4	1.0	1.0	1.0
h_3, h_4, h_5	4.75			
h_6	5.0			

2.2. Finite element simulations

All simulations were performed with the finite element code Zebulon. 3D meshes were constructed following the same mesh refinement strategy as in [3]. This mesh design has been proved to provide extremely accurate solutions for several axisymmetric [14,15] and 3D [16] contact problems dealing with both, sharp and spherical indentation experiments. A typical finite element model in the present simulations contains about 21200 eight-node linear brick elements (c3d8), and consists of various zones of different element density, connected through a structured transition region optimized to minimize the distortion of field variables within the plastic zone (see Fig. 1). The simulations are conducted under displacement control so that maximum penetration depth is kept constant in all cases ($h_s^{max} = 3.5$ μm). This ensures that the maximum contact radius remains always smaller than $L/50$, being L the radial dimension of the cylindrical sample. This condition minimizes the specimen's boundary effect and allows for the recovery of the Boussinesq's solution far away from the contact area [16].

Only well defined crystallographic planes were indented in order to take advantage from the partial symmetry of the resulting contact configurations. Following this modeling strategy, only reduced portions of the crystal sample actually need to be explicitly modeled by applying pertinent boundary conditions at the corresponding symmetry planes. From this procedure, complete information of the full 3D deformation patterns can be actually obtained at a lower computational cost. One of the finite element

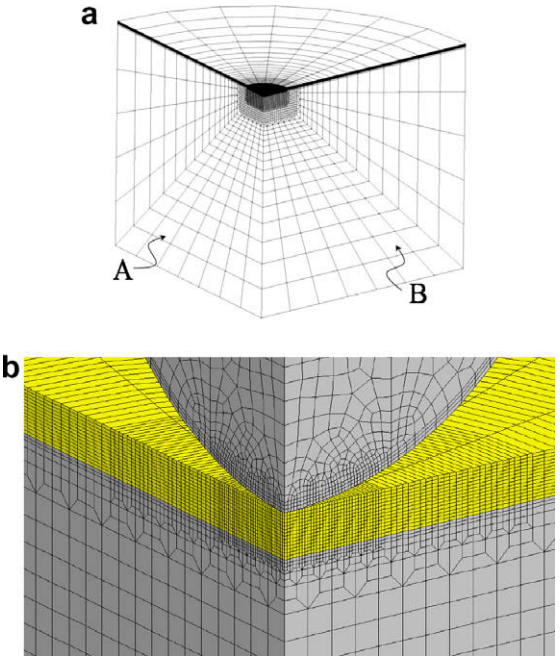

Fig. 1. Cross sectional view of one of the models used in the simulations. A detail of the mesh close to the contact zone is shown in (b) where the coating region appears in yellow. (For interpretation of the references to colour in this figure legend, the reader is referred to the web version of this article.)

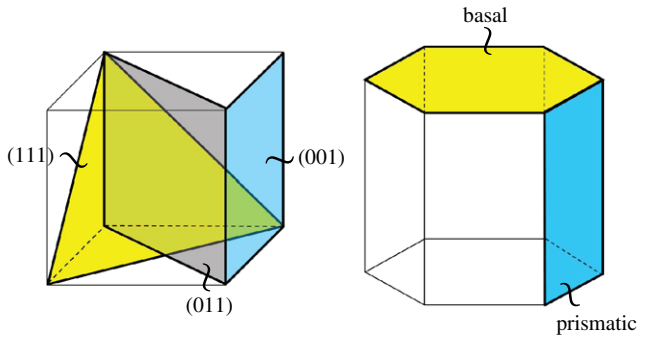

Fig. 2. Copper and zinc crystallographic planes indented in the finite element simulations of the present work concerning crystal plasticity. (001), (011) and (111) planes were chosen for f.c.c crystals while (0001) basal and $(1\bar{1}00)$ prismatic planes were simulated in the h.c.p case. For the simulations concerning perfectly elastic solids, some additional planes were considered for completeness (i.e. the the twinning plane $(10\bar{1}2)$ and the pyramidal planes $(10\bar{1}1)$ and $(11\bar{2}2)$ in h.c.p crystals, and a randomly oriented plane (632) in f.c.c crystals.

meshes used in the simulations is shown for instance in Fig. 1. In this particular case, the model encompasses a 90° sector of the crystal sample and was used on indentations performed in (001) copper planes. In order to satisfy the symmetry of the resulting contact configuration, displacements perpendicular to cross-section symmetry planes were precluded for all nodes lying on the boundaries (A and B in the figure). Similar modeling strategies were used, when possible, for all orientations and crystal structures. Indented crystal planes are indicated in Fig. 2 for f.c.c copper and h.c.p zinc crystals. Some additional planes, including non-symmetric orientations, were also indented for completeness in the case of perfectly elastic anisotropic contact problems (see Section 3.1). In this case, full 3D models (360°) could be used due to the small computational cost of the elastic simulations.

3. Results and discussion

3.1. Elastic anisotropic contact response

For the sake of comparison, the purely elastic contact problem was first studied. Fig. 3a and b shows the P–h_s curves obtained from the simulations of spherical indentation on various crystallographic planes of idealized solids, that exhibit the anisotropic perfectly elastic properties of copper and zinc single crystals, respectively. It can be observed that P–h_s curves constitute a sensible measure of the elastic properties of the crystal along the direction perpendicular to the indented plane. Note for instance, that the (111) and the (001) planes of the f.c.c. crystal exhibit the stiffer and the more compliant contact responses, respectively. This correlates well with the fact that the highest and lowest values of Young's modulus are also found along these two directions when copper single crystals are uniaxially tested within the elastic regime. Similar results hold for the ideally elastic hexagonal crystal in Fig. 3b. In this case, indentation along the c-crystal axis exhibits the softest response, which is in agreement with the small Young's modulus manifested by pure zinc crystals uniaxially tested along this direction.

Nevertheless, contact behavior actually results in a somehow averaged response over all possible uniaxial directions. Hence, contact anisotropy that is quantified herein as the relative difference in the P–h_s curves, is less significant as compared to the ratio between the Young's modulus uniaxially measured along the corresponding crystallographic directions. In this sense, note that for ideally elastic copper crystals, the ratio between the applied load in the (111) and (001) planes for a given penetration depth is

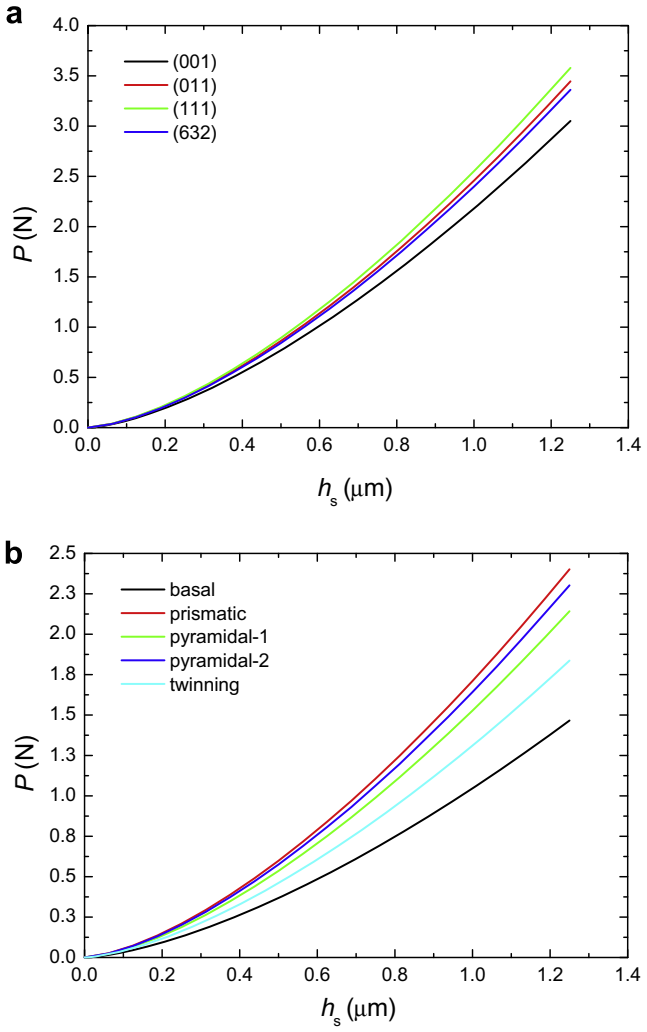

Fig. 3. P–h_s curves obtained from the simulations of spherical indentation ($R = 100$ μm) experiments conducted on different crystallographic planes of a perfectly elastic solid exhibiting the elastic properties of copper (a) and zinc (b) single crystals.

equal to $P_{111}/P_{001} = 1.15$, while the corresponding ratio of Young's modulus in these directions is equal to $E_{111}/E_{001} = 2.87$. Similar observations hold true for the h.c.p. crystal with the elastic properties of zinc.

The elastic contact anisotropy of single crystals could be also advanced from the different shape and size of the stress fields developed within crystals indented with a homogeneous spherical indenter. Such stress fields can be observed in Fig. 4, where the influence of crystal orientation upon stress concentration becomes evident. It is also interesting to note that the stress fields within the indenter, which is assumed to behave as an isotropic elastic solid, closely reproduce those predicted from the solution of the Hertz contact problem [17]. The solution within the indenter thus remains almost unchanged irrespectively of the actual orientation of the indented crystal.

3.2. Elasto-plastic anisotropic contact response

The triaxially dominant character of indentation-stress fields facilitates the activation of all admissible slip systems in elasto-plastic crystals. Similarly to the perfectly elastic case, this results in a significant homogenization of the contact response. Nevertheless, the contact behavior becomes much more complex when the

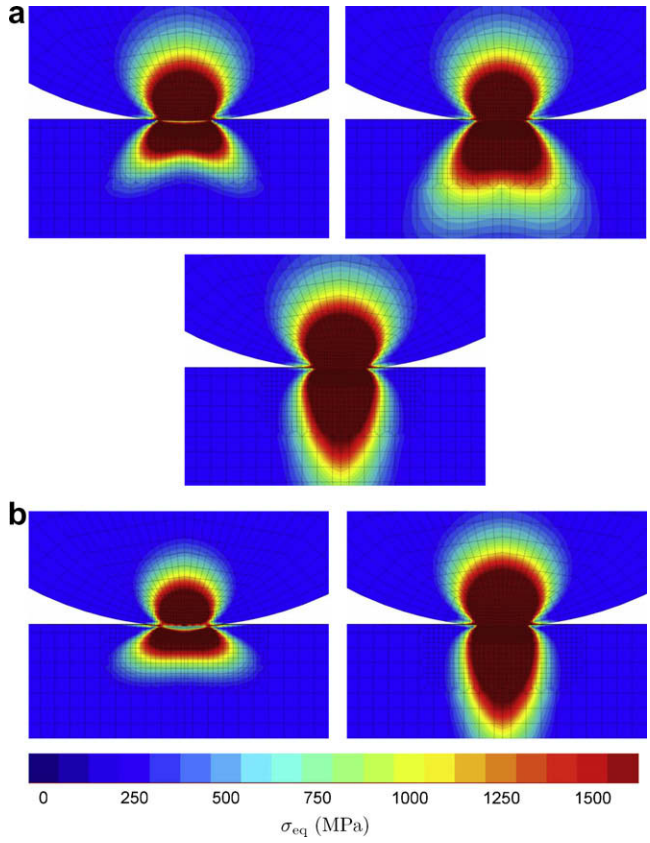

Fig. 4. Equivalent von Mises stress fields from the simulations of spherical indentation experiments on idealized f.c.c (a) and h.c.p (b) crystals with the elastic properties of copper and zinc. The present symmetric configurations arise when indenting the (001), (011) and (111) (a) and the basal and prismatic (b) crystallographic planes of the f.c.c and the h.c.p crystals, respectively. Penetration depth in present figure is $h_s = 1.25$ μm.

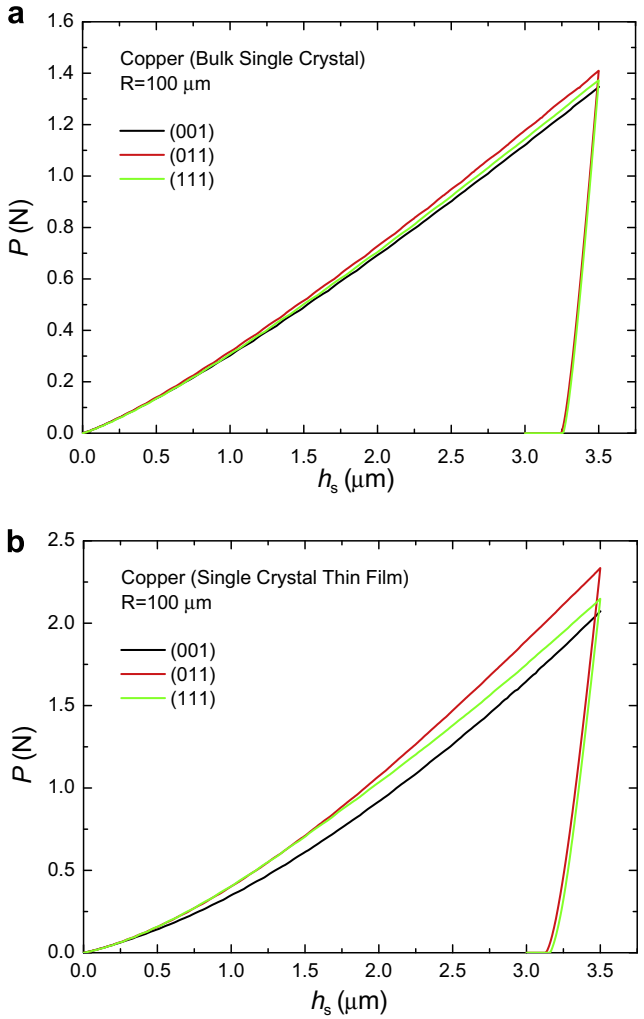

Fig. 5. P–h_s curves of bulk (a) and thin film (b) copper single crystals indented on different crystallographic planes with a spherical indenter of radius $R = 100$ μm. Film thickness $t = 14$ μm.

fully plastic contact regime is gradually attained as indentation proceeds. Figs. 5 and 6 shows the P–h_s curves of bulk (a) and thin film (b) copper and zinc single crystals indented on different crystallographic planes with a spherical indenter of radius R = 100 μm. It can be observed that in both cases, the degree of anisotropy inferred from instrumented indentation curves of bulk materials decreases as compared to the corresponding purely elastic problem. For bulk copper, such a reduction results in a maximum ratio of indentation loads $P_{011}/P_{001} = 1.05$, which is sensibly smaller as compared to the value $P_{111}/P_{001} = 1.15$ in the perfectly elastic case. At this point, it must be noted that (111) is the stiffest plane when indenting elasto–plastic bulk copper crystals with sharp indenters (see [4]). Although this is also the case when indenting the perfectly elastic solid (see Fig. 2a) with a spherical tip, it does not longer holds true when indenting bulk copper crystals with such an indenter's geometry (see Fig. 5). In this case, (011) appears to be the stiffest plane, thus suggesting a distinct plastic deformation development depending on the actual indenter geometry.

For elasto-plastic zinc crystals, a ratio $P_{pris}/P_{bas} = 1.10$ is observed in front of the maximum value $P_{pris}/P_{bas} = 1.45$ encountered for the idealized perfectly elastic solid. It is also important to remark that contact anisotropy is enhanced again when the influence of an elastic substrate comes into play. At a maximum penetration depth $h_s = 3.5$ μm, the 14 μm-thick thin film of copper single crystal simulated in the present work, shows a contact anisotropy similar to that of perfectly elastic bulk crystals. Nevertheless, it is even more significant that the relative compliance of different indented planes does not remain constant. In other words, as indentation proceeds, the corresponding indentation load increases at different rates depending on the actual indented plane. This becomes evident in Fig. 6 for the case of Zn. In this case, even the order of the P–h_s curves becomes quickly reversed, so that the basal plane rapidly becomes stiffer than the prismatic one due to the presence of the elastic substrate. This is due to the fact that, for zinc crystals indented along the c-axis, the plastic zone grows completely elongated along the vertical direction. It promotes a strong and quick interaction of the growing plastic zone with the elastic substrate (see Fig. 9b). On the contrary, the plastic zone within Zn crystals indented along the direction perpendicular to the prismatic plane grows predominantly parallel to the surface. For this reason, in such a configuration the interaction with the substrate is differed to larger penetration depths (see Fig. 9d).

An additional complexity in the interpretation of the contact behavior arises from the non self-similar nature of spherical indenters. The contact regime attained beneath a spherical tip evolves as plastic deformation increases with the penetration depth [18]. For elasto-plastic anisotropic single crystals, such an evolution of the contact regime can be taken as an additional explanation of the distinct order of P–h_s curves in copper crystals indented with sharp or spherical indenters. In the former case, (111) appears to be the stiffest plane, and by virtue of self-similar arguments it remains the same for any given penetration depth [4]. On the contrary, simulations in the present work show that for spherical

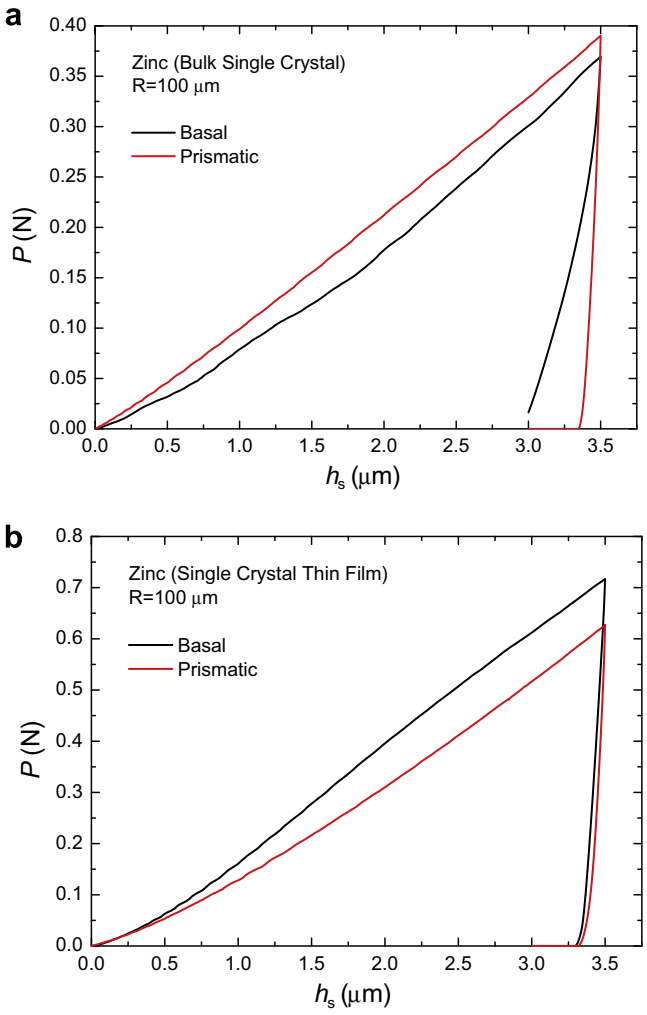

Fig. 6. P–h_s curves of bulk (a) and thin film (b) zinc single crystals indented on different crystallographic planes with a spherical indenter of radius $R = 100$ μm. Film thickness $t = 14$ μm.

indenters, (1 1 1) is the stiffest plane only at the very beginning of the experiment, but (0 1 1) becomes stiffer at larger penetration depths.

The analysis of the anisotropy in spherical contact problems can be better characterized by the evolution of the nominal hardness (H_s) as a function of the indentation ratio (h_s/R), instead of the P–h_s curve itself. The assessment of the nominal hardness from an instrumented indentation experiment is straightforward. It can be simply computed as the ratio between the applied load (P) and the projected contact area associated to the penetration depth (h_s), disregarding pile up or sinking-in effects. Fig. 7 shows such an evolution for different indented crystallographic planes of copper single crystals. Various sets of data are plotted, each one concerning different film thickness (t) over indenter radius (R) ratios. In this way, the above mentioned evolution of contact anisotropy for non self-similar contacts becomes evident. For very shallow penetrations, spherical indentation exhibits a purely elastic response similar to the solution of the isotropic Hertz contact problem. As long as penetration depth increases, plastic deformation comes into play. It causes a continuous evolution of contact anisotropy, which is distinctly affected by the elastic substrate depending on the actual indented plane. We can see, for instance, that the rate of increase of nominal hardness is smaller for the (1 1 1) plane, so that its highest value of hardness at low penetration depth ratios becomes the smallest one at higher ratios.

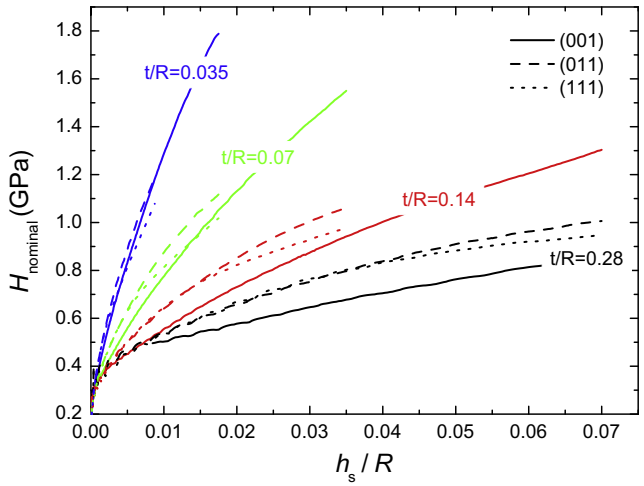

Fig. 7. Nominal hardness as a function of the penetration depth ratio (h_s/R) for different indented planes of copper single crystals. Various sets of data are plotted concerning different ratios of coating thickness (t) over indenter radius (R).

3.3. Plastic zone morphology

The size and morphology of the plastic zone are characteristic features of indentation experiments. They allow for an estimation of the yield strength and for the assessment of the substrate influence on the contact response of coatings and thin films [18–20]. Plastic zone morphology is also one key issue on the assessment of contact anisotropy, since the actual development of the plastic zone can be largely influenced by the orientation of the indented crystallographic plane [4,5]. Hence, contact behavior may be better understood in light of the results concerning plastic zone development. The finite element simulations within the context of the present crystal plasticity model, allow us for the assessment of a detailed description of single crystal plastic zones, and to attempt the correlation between characteristic plastic zone features and contact anisotropy. Figs. 8 and 9 show detailed pictures of the plastic zones developed on copper and zinc single crystals respectively. Figs. 8a, c and e correspond to bulk copper crystals indented along ⟨0 0 1⟩, ⟨0 1 1⟩ and ⟨1 1 1⟩, respectively, while (b), (d) and (f) concern their thin film counterparts. Visualization of the cumulated plastic strain on all active slip systems ($\sum_i v^i$) shows that plastic deformation is largely heterogeneous for bulk single crystals and it always concentrates along the slip system directions. Furthermore, significant differences arise for various crystal orientations: (0 0 1) plane exhibits a more localized plastic zone just below the contact area. On the contrary the (1 1 1) plane exhibits a plastic zone which is slightly more extended, thus covering a wider area with a smoother deformation gradient.

Even more significant differences can be observed in zinc single crystals. Figs. 9a and c shows the plastic zones of bulk crystals indented along the directions perpendicular to the basal and prismatic planes, respectively. In the former case, plastic deformation progresses perpendicular to the indented plane. This is due to the fact that the initial orientation of the basal plane, combined with the predominant compressive stress at the contact zone, results in a small Schmid factor for the basal slip system family. On the contrary, prismatic and pyramidal slip systems become favored for the development of plastic strain. Such a *coarse-grain* picture of slip system activations results in a plastic zone that is elongated along the through-thickness direction of the indented crystal. For indentations conducted on the basal plane, strain localization is observed all around the contact boundary in the form of a circular ring at the free surface of the crystal (see Fig. 9a). Such a

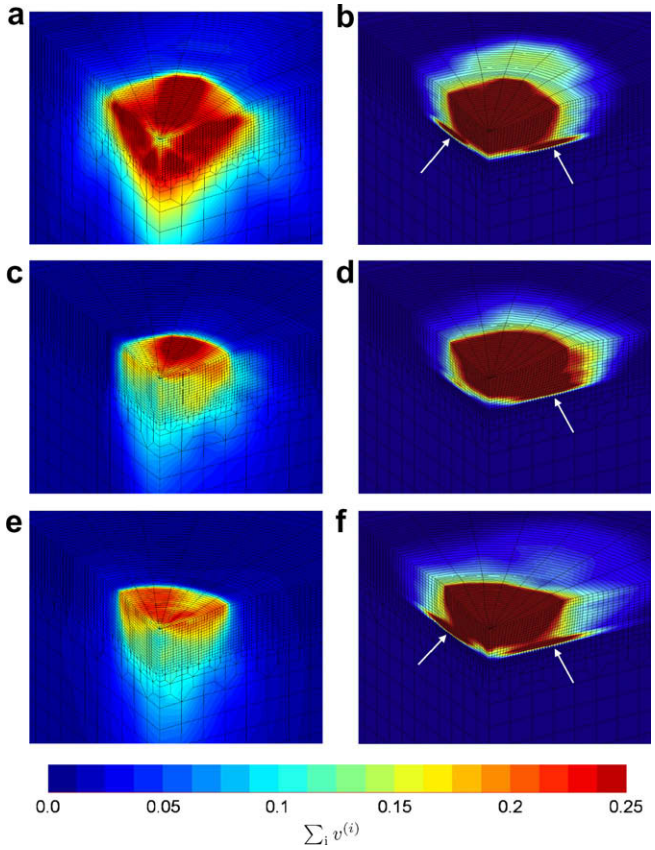

Fig. 8. Details of the indentation-induced plastic zone in the simulations concerning f.c.c copper crystals. (a), (c) and (e) correspond to the (001), (011) and (111) indented planes of bulk crystals. (b), (d) and (f) correspond to their thin film counterparts. Plastic zone is assessed by considering the total cumulated plastic strain variable. The upper visualization limit was adjusted to 25% in order to discern the main features of plastic deformation distribution. White arrows point to the specific locations where high plastic strain localization occurs within the coating–substrate interface. Penetration depth in the figures is $h_s = 3.5\ \mu m$.

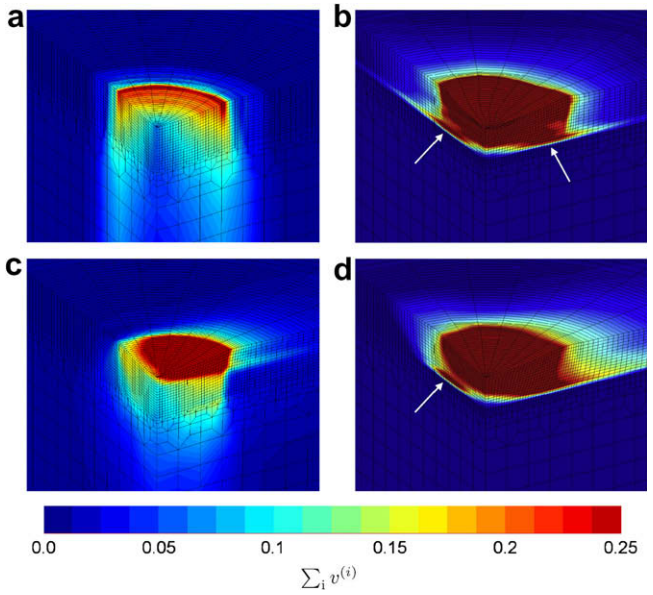

Fig. 9. Details of the indentation–induced plastic zone in the simulations concerning h.c.p zinc crystals. (a) and (c) correspond to the basal and prismatic indented planes of bulk crystals. (b) and (d) correspond to their thin film counterparts. The upper visualization limit was adjusted to 25% in order to discern the main features of plastic deformation distribution. White arrows point to the specific locations where high plastic strain localization occurs within the coating–substrate interface. Penetration depth in the figures is $h_s = 3.5\ \mu m$.

characteristic feature of the deformation pattern would promote plastic damage, and further nucleation of circular cracks similar to those which are often observed to propagate during indentation experiments in polycrystals [21,22].

Fig. 9c, which corresponds to a zinc crystal indented perpendicular to the prismatic plane, shows a plastic zone that develops parallel to the indented surface. In this case, plastic strain appears to be much more homogeneous beneath the indenter. Nevertheless, there still exists an important anisotropy that results in a very elongated plastic zone. Again, this is due to the preferential plastic strain localization along the slip direction lying on the indented surface and the otherwise reduced deformation that occurs along the perpendicular in-surface direction. As it will be seen in Fig. 11c, such an elongated pattern becomes also evident when attention is directed to the indentation imprint.

As it is expected, the presence of an elastic substrate constrains the deformation of the coating, thus increasing the stress level necessary for continuing the plastic flow. It also promotes a large localization of the deformation beneath the indenter and a growing plastic zone along directions parallel to the surface. This can be observed in Figs. 8b, d and f for (001), (011) and (111)-oriented thin film copper crystals, respectively, and in Figs. 9b and d for both basal and prismatic-oriented zinc single crystal thin films. Furthermore, a significant outcome from the simulations are the characteristic features of plastic strain localization that appear in particular regions within the coating-substrate interface (see white arrows in Figs. 8 and 9). Those specific locations always correspond to the intersection of through-thickness slip directions with the substrate, and they constitute potential areas for delamination and failure of the films.

3.4. Surface deformation patterns and indentation imprint morphology: pile up or sinking-in

Indentation experiments have been used since a long time for the evaluation of mechanical properties from their correlation with contact parameters assessed from very small volumes of material. Nevertheless, the non-uniqueness in the solution of such an inverse correlation problem seriously hampers an accurate estimation of properties [3]. The actual deformation mode developing around the indentation imprint (i.e. pile up or sinking-in) has been identified as a key point for the unique identification of the correct solution. Because of this, the analysis of imprint deformation patterns for different crystal orientations is undertaken. The influence of quasi-rigid substrates on these characteristic deformation features is addressed as well.

Figs. 10 and 11 shows the vertical displacement close to the indentation zone. For the case of copper (see Fig. 10), it can be observed that surface deformation is not homogeneous for different simulations, neither all around the contact perimeter for a given indented plane. Although pile up always occurs in bulk copper, it almost vanishes for the (111) plane. In fact, pile up in bulk copper crystals actually appears only slightly away from the contact boundary, and just at specific locations that correspond to those positions towards which slip directions point to. The material actually sinks-in at the precise position of the contact boundary and all over extended areas far away from slip directions. In the extreme case of indentations conducted on the (111) plane of bulk copper crystals, the pile up almost entirely disappears. This suggests that bulk crystals predominantly undergo material sinking-in around the indenter. Although the actual surface deformation behavior strongly depends on the hardening capacity of materials [23], the

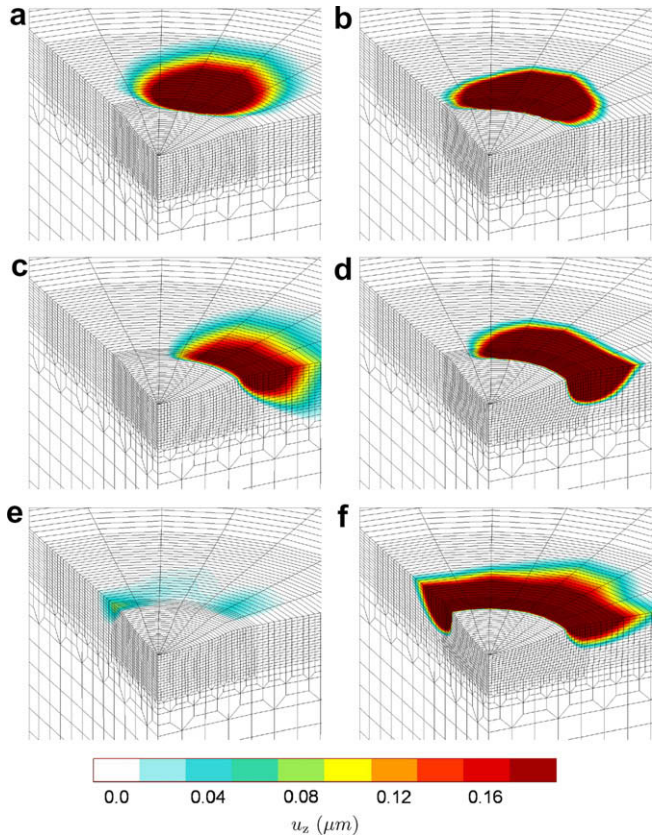

Fig. 10. Vertical displacement of the material close to the contact zone. Actual penetration depth is $h_s = 3.5$ μm. (a), (c) and (e) correspond to the (0 0 1), (0 1 1) and (1 1 1) indented planes of bulk copper crystals. (b), (d) and (f) correspond to their thin film counterparts. Colored areas correspond to positive displacements thus denoting pile up regions. (For interpretation of the references to colour in this figure legend, the reader is referred to the web version of this article.)

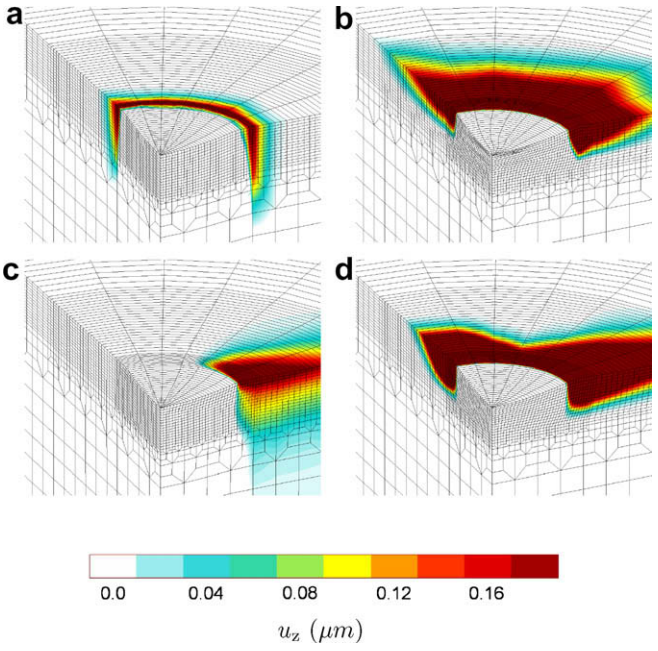

Fig. 11. Vertical displacement of the material close to the contact zone. Actual penetration depth is $h_s = 3.5$ μm. (a) and (c) correspond to the basal and prismatic indented planes of bulk zinc crystals. (b) and (d) correspond to their thin film counterparts. Colored areas correspond to positive displacements thus denoting pile up regions. (For interpretation of the references to colour in this figure legend, the reader is referred to the web version of this article.)

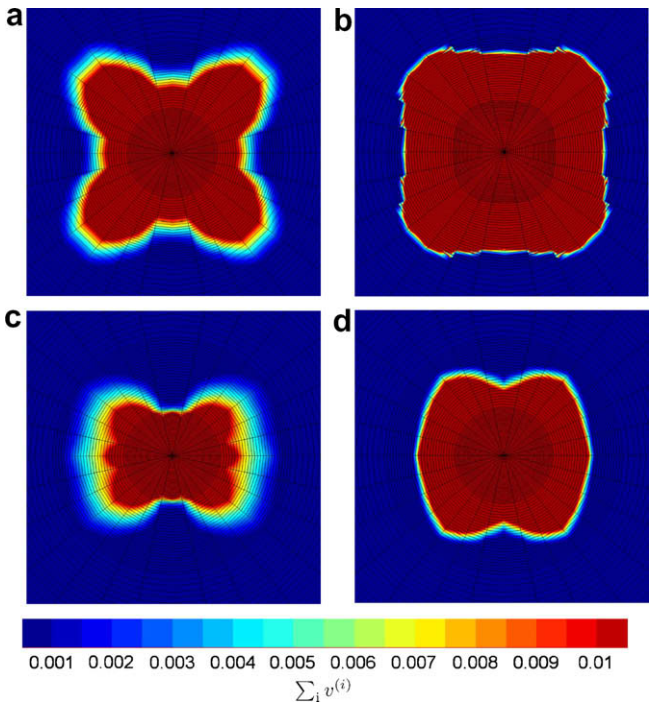

Fig. 12. Top view of the plastic zone emerging at the free surface of f.c.c copper crystals. Visualization limits were adjusted to better capture the whole plastic zone. (a) and (c) correspond to the (0 0 1) and (0 1 1) indented planes of bulk crystals while (b) and (d) correspond to their thin film counterparts.

above results for copper single crystals seem to be consonant with those concerning well-annealed polycrystalline cooper [4]. As it could be expected, the additional constraint introduced by the elastic substrate in thin film systems, enhances material pile up. Since the elastic substrate is much more rigid than the coating, plastic flow must inevitably occur towards the free surface thus promoting extensive pile up around the indentation imprint. It is interesting to note that such an effect is even more pronounced for the (1 1 1) indented plane. Consequently, this particular orientation manifests the strongest sinking-in/pile up contrast between bulk and thin film systems.

The anisotropy in the surface deformation between different indented planes becomes more evident in h.c.p crystals. First, it can be observed that when the basal plane is indented, an homogeneous pile up occurs within a narrow ring all around the contact boundary (see Fig. 11a). By contrast, the surface deformation that develops when indenting the h.c.p crystal on the prismatic plane shows and extremely directional pattern (see Fig. 11c); significant pile up develops along the slip direction located at the free surface while extensive sinking-in occurs along the corresponding orthogonal direction. As in the case of copper crystals, the presence of a quasi-rigid substrate enhances material pile up all around the contact periphery.

The influence of the substrate on the indentation imprint morphology actually depends on the crystallographic structure of the indented material. This distinct effect on the imprint can be better observed by directing attention to the plastic zone morphology when it comes to the free surface. Fig. 12 shows top views of such a plastic zone for bulk (a) and (c) and thin film (b) and (d) copper single crystals. (a) and (b) pertain to simulations of single crystals indented along ⟨0 0 1⟩ directions while (c) and (d) correspond to the (0 1 1) indented plane. They show that in both cases, the in-surface plastic zone of bulk single crystals is more anisotropic, and per-

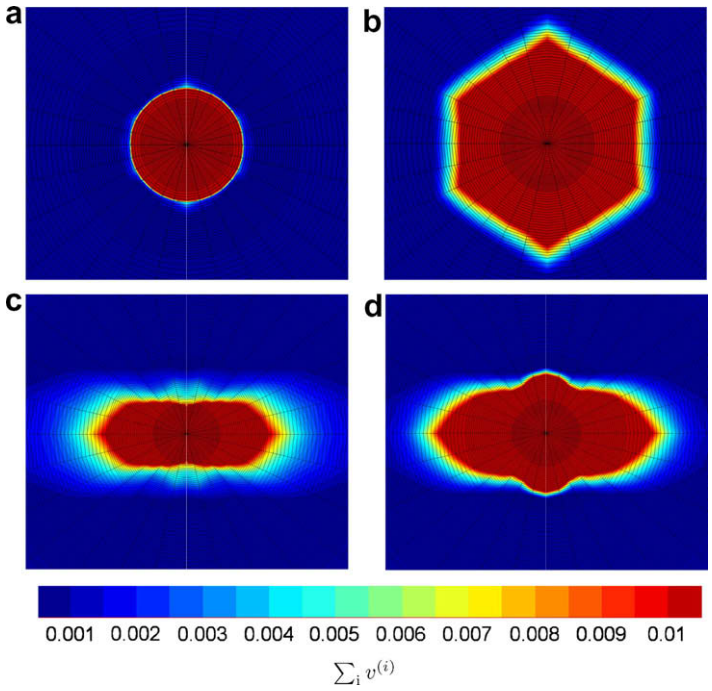

Fig. 13. Top view of the plastic zone emerging at the free surface of h.c.p zinc crystals. Visualization limits were adjusted to better capture the whole plastic zone. (a) and (c) correspond to the basal and prismatic indented planes of bulk crystals while (b) and (d) correspond to their thin film counterparts.

fectly trace the deformation along the plastic slip directions across the surface. On the other hand, the corresponding thin film plastic zones tend to be more homogeneous and to mask those slip system traces. By contrast, such a description of the surface deformation does not hold in the case of zinc. In spite of the large plastic anisotropy of h.c.p crystals, the surface deformation pattern on the basal plane denotes transverse isotropic behavior. This is corroborated through inspection of the plastic zone at the surface of an indentation conducted on such a basal plane. As it is shown in Fig. 13a the plastic zone at the free surface level results to be perfectly circular. On the other hand, the constraining action of an elastic substrate clearly reveals the hexagonal symmetry of zinc crystals (see Fig. 13b). Hence, we see that, concerning the effect of substrate constrainment on the surface deformation evolution, zinc single crystals indented along the *c*-axis behave just the opposite to copper crystals. Finally, indentations performed on the prismatic plane does not show a significant difference on the shape of the in-surface plastic zone between bulk and thin film zinc crystals. Hence, for this particular orientation the substrate only affects the magnitude of the plastic strain and its extension but not the shape of the plastic zone on the indented surface.

3.5. Conclusions

The finite element simulations in the present work allowed us to analyze the anisotropic contact behavior of f.c.c and h.c.p bulk single crystals and thin films on hard substrates. The following are the main findings of the research.

(i) At first, the anisotropy in the contact response was analyzed in terms of the instrumented indentation $P-h_s$ curves. In spite of the intrinsic anisotropy of the single crystal plastic flow, indentation load evolution appears to be quite homogeneous in f.c.c bulk copper crystals. This is attributed to the combination of the highly triaxial character of the indentation induced stress field, and the large number of equivalent slip systems available through the f.c.c octahedral family of slip systems. By contrast, the contact response results to be more anisotropic when h.c.p zinc crystals are indented. This is due to the small number of available slip systems in the h.c.p structure as well as to the heterogeneity of plastic properties within different families of slip systems.

(ii) Second, the influence of a hard substrate largely enhances contact anisotropy, thus suggesting an orientation-dependent interaction of the growing plastic zone with the substrate. This is particularly evident in the case of zinc crystals, for which a very elongated plastic zone develops along the *c*-axis when indenting the basal plane. Such a highly directional plastic zone promotes a very strong and quick interaction with the substrate, so that indentation load immediately rises for this particular orientation.

(iii) Next, the size and shape of the plastic zone beneath the indenter has been systematically studied for different crystal orientations. It has been observed that the plastic zone preferentially grows along the slip system directions. As a result, in coated systems, a strong localization of plastic deformation occurs at those specific points where slip system directions intersect the substrate. Due to the accumulation of plastic damage, these specific areas are prone to crack nucleation. The identification of these points is relevant for the prediction of potential delamination and failure of the coatings.

(iv) At last, the analysis of imprint morphology and surface deformation modes has been addressed. For a given indented plane, the pile up or sinking-in patterns are very anisotropic. The only exception occurs in h.c.p crystals indented along the *c*-axis, in which case surface deformation appears to be transversely isotropic. Finally, it has been shown that hard substrates significantly enhance the material pile up, although the influence is again dependent of the actual orientation of the indented crystal. Such a complex anisotropic behavior of the surface deformation may be expected to challenge the evaluation of mechanical properties from micro-hardness tests.

Acknowledgement

We gratefully acknowledge financial support from the European Commission through the Marie-Curie Research Training Network SizeDepEn (Contract No. MRTN-CT-2003-504634).

References

[1] M. Dao, N. Chollacoop, K.J. Van Vliet, T.A. Venkatesh, S. Suresh, Acta Mater. 49 (19) (2001) 3899–3918.
[2] L. Wang, S.I. Rokhlin, J. Mater. Res. 21 (4) (2006) 995–1011.
[3] O. Casals, J. Alcalá, Acta Mater. 53 (13) (2005) 3545–3561.
[4] O. Casals, J. Očenášek, J. Alcalá, Acta Mater. 55 (1) (2007) 55–68.
[5] Y. Wang, D. Raabe, C. Klüber, F. Roters, Acta Mater. 52 (2004) 2229–2238.
[6] Y. Liu, B. Wang, M. Yoshino, S. Roy, R. Komanduri, J. Mech. Phys. Sol. 53 (12) (2005) 2718–2741.
[7] T. Zhu, J. Li, K.J. Van Vliet, S. Ogata, S. Yip, S. Suresh, J. Mech. Phys. Sol. 52 (3) (2004) 691–724.
[8] M.C. Fivel, C.F. Robertson, G.R. Canova, L. Boulanger, Acta Mater. 46 (17) (1998) 6183–6194.
[9] L. Méric, P. Poubanne, G. Cailletaud, J. Eng. Mater. Technol. 113 (1991) 162–170.
[10] R.J. Asaro, Adv. Appl. Mech. 23 (1983) 1–115.
[11] F. Šiška, S. Forest, P. Gumbsch, D. Weygand, Modelling Simul. Mater. Sci. Eng. 14 (2006) 1–22.
[12] R. Parisot, S. Forest, A.-F. Gourgues, A. Pineau, D. Mareuse, Comput. Mater. Sci. 19 (1–4) (2000) 189–204.
[13] R. Parisot, S. Forest, A. Pineau, F. Grillon, X. Démonet, J.-M. Mataigne, Metal. Mater. Trans. 35A (2004) 797–811.
[14] R. Hill, B. Storåkers, A.B. Zdunek, Proc. R. Soc. Lond. (423) (1989) 301–330.
[15] M. Mata, J. Alcalá, J. Mater. Res. 18 (7) (2003) 1705–1709.
[16] A.E. Giannakopoulos, P. L Larsson, R. Vestergaard, Int. J. Solids Struct. 31 (19) (1994) 2679–2708.
[17] K.L. Johnson, Contact Mechanics, Cambridge University Press, Cambridge, 1985.
[18] M. Mata, O. Casals, J. Alcalá, Int. J. Solids Struct. 43 (20) (2006) 5994–6013.
[19] D. Kramer, H. Huang, M. Kriese, J. Robach, J. Nelson, A. Wright, D. Bahr, W.W. Gerberich, Acta Mater. 47 (1999) 333–343.
[20] C.L. Woodcock, D.F. Bahr, Scr. Mater. 43 (2000) 783–788.
[21] E.A. Pérez, R.M. Souza, Surf. Coat. Technol. (188–189) (2004) 572–580.
[22] G. Geandier, S. Denis, A. Hazotte, A. Mocellin, J. Eur. Ceram. Soc. 25 (2005) 1119–1132.
[23] J. Alcalá, A.C. Barone, M. Anglada, Acta Mater. 48 (13) (2000) 3451–3464.